



**UNIVERSITI PUTRA MALAYSIA**

***MODELLING THE DYNAMICS AND CONTROL SYSTEM OF HYBRID  
AIRSHIP UAV (HAU-3)***

**MOHD FAZRI BIN SEDAN**

**FK 2022 21**



**MODELLING THE DYNAMICS AND CONTROL SYSTEM OF HYBRID  
AIRSHIP UAV (HAU-3)**

**By**

**MOHD FAZRI BIN SEDAN**

**Thesis Submitted to the School of Graduate Studies, Universiti Putra  
Malaysia, in Fulfilment of the Requirements for the Degree of Master of  
Science**

**April 2022**

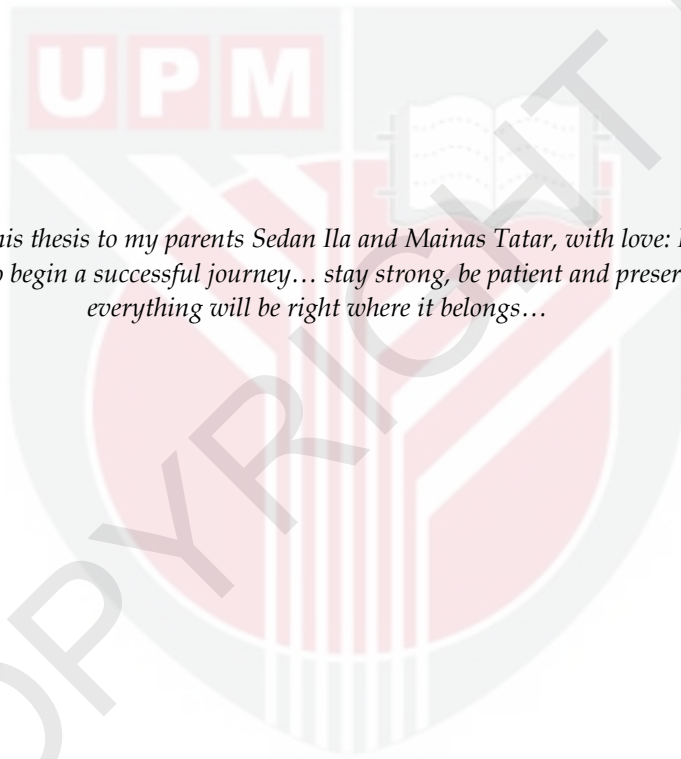
All material contained within the thesis, including without limitation text, logos, icons, photographs and all other artwork, is copyright material of Universiti Putra Malaysia unless otherwise stated. Use may be made of any material contained within the thesis for non-commercial purposes from the copyright holder. Commercial use of material may only be made with the express, prior, written permission of Universiti Putra Malaysia.

Copyright © Universiti Putra Malaysia



## DEDICATIONS

*I dedicated this thesis to my parents Sedan Ila and Mainas Tatar, with love: It takes a single step to begin a successful journey... stay strong, be patient and preserved, and everything will be right where it belongs...*



Abstract of thesis presented to the Senate of Universiti Putra Malaysia in  
fulfilment of the requirement for the degree of Master of Science

## **MODELLING THE DYNAMICS AND CONTROL SYSTEM OF HYBRID AIRSHIP UAV (HAU-3)**

By

**MOHD FAZRI BIN SEDAN**

**April 2022**

**Chair : Ahmad Salahuddin Mohd Harithuddin, PhD**  
**Faculty : Engineering**

In this thesis, a 3.3 m length, finless hull airship called HAU-3 is presented. Four vector thrusters arranged in H-Frame configurations were attached to the hull, which enable the airship to maneuver in 5DOF. To allow a deeper understanding of the HAU-3 motion behavior and to design a flight controller, a reliable dynamics model representation and simulator of HAU-3 are developed. A six-degrees of freedom (6DOF) non-linear mathematical model representation is constructed using the Newton-Euler approach. The dynamics model parameters were identified via semi-empirical, computer-aided modelling (CAD) and experimental approaches. The HAU-3 dynamics model was then integrated into Simulink and MATLAB to construct a closed-loop simulator to analyze the airship's behavior. Five separate Proportional, Integral and Derivative (PID) controllers were designed using the developed non-linear dynamic model. A series of indoor static tests and outdoor flight tests were conducted to evaluate the controller performance and to validate the simulator response. A dynamic response model of the vector thrusters developed provides excellent agreement with the actual thrust and motor transient response with 0.29 s delay and 0.2 N steady-state error. The indoor static test of the yaw controller shows an adequate yaw state change tracking performance with a 9.5% average difference in maximum overshoot and approximately 30% settling time difference by comparison of actual and simulated responses. The controller is able to suppress the pendulum oscillation in pitch and roll with 0.165 Hz and 0.3 Hz oscillation frequency, respectively and at least 20° maximum angle deviation. The altitude controller also shows an excellent performance in tracking the change in altitude

during outdoor flight tests with an average 0.5 m altitude difference between simulation and actual recorded altitude. The developed HAU-3 simulator provides a reasonable estimate of the airship's attitude and translational states for modelling and simulation purposes.



Abstrak tesis yang dikemukakan kepada Senat Universiti Putra Malaysia  
sebagai memenuhi keperluan untuk Ijazah Master Sains

## PEMODELAN DINAMIK DAN SISTEM KAWALAN UAV PESAWAT HIBRID (HAU-3)

Oleh

MOHD FAZRI BIN SEDAN

April 2022

**Pengerusi : Ahmad Salahuddin bin Mohd Harithuddin, PhD**  
**Fakulti : Kejuruteraan**

Tesis ini membincangkan mengenai sebuah pesawat tanpa sirip sepanjang 3.3 meter yang dikenali sebagai HAU-3. Empat penjujukan vektor yang disusun dalam konfigurasi H-Frame telah dipasang pada badan pesawat yang membolehkan pesawat bergerak dalam sistem 5DOF. Bagi pemahaman yang lebih mendalam tentang tingkah laku gerakan HAU-3 dan bagi tujuan mereka bentuk alat pengawal penerbangan, perwakilan model dinamik yang boleh dipercayai dan simulator HAU-3 dibangunkan. Perwakilan model matematik bukan linear enam darjah kebebasan (6DOF) dibina menggunakan pendekatan Newton-Euler. Parameter model dinamik dikenal pasti melalui pendekatan semi-empirikal, reka bentuk berbantu komputer (CAD) dan eksperimen. Model dinamik HAU-3 kemudiannya disepadukan ke dalam Simulink dan MATLAB untuk membina simulator gelung selanjur rapat untuk menganalisis tingkah laku pesawat. Lima alat kawalan *Proportional, Integral dan Derivative (PID)* berasingan telah direka bentuk menggunakan model dinamik bukan linear yang telah dibangunkan. Satu siri ujian statik dalaman dan ujian penerbangan luar telah dijalankan untuk menilai prestasi alat kawalan dan untuk mengesahkan tindak balas simulator. Model tindak balas dinamik penjujukan vektor yang dibangunkan memberikan keserasian yang sangat baik dengan tujuh sebenar dan motor sambutan fana dengan lengah 0.29s dan ralat keadaan mantap 0.2 N. Ujian statik dalaman alat kawalan rewang menunjukkan prestasi pemacu perubahan keadaan rewang yang mencukupi dengan perbezaan purata 9.5% dalam melewati maksimum dan kira-kira 30% perbezaan masa enapan dengan perbandingan tindak balas simulasi dan tindak balas sebenar. Alat kawalan mampu menahan ayunan bandul dalam anggul dan beroleng dengan ayunan 0.165 H dan 0.3 Hz frekuensi

ayunan masing-masing sekurang-kurangnya  $20^\circ$  sudut sisihan maksimum. Alat kawalan altitud juga menunjukkan prestasi cemerlang dalam menjejaki perubahan altitud semasa ujian penerbangan luar dengan purata perbezaan ketinggian 0.5 m antara simulasi dan ketinggian sebenar yang direkodkan. Simulator HAU-3 yang dibangunkan menyertakan anggaran yang munasabah tentang sikap pesawat dan keadaan translasi untuk tujuan pemodelan dan simulasi.





## ACKNOWLEDGEMENT

Thank you to The Almighty, Allah S.W.T for giving me the strength and willpower to complete this research and thesis. First, I would like to take this opportunity to express my gratitude to the individuals who contributed to the completion of this research work and inspired me during the up and down of this journey. Foremost, thanks to my beloved family who always be there to give me moral support throughout my Master's Studies. Without them, it is impossible for me to achieve this stage.

My special gratitude to Dr Ahmad Salahuddin Mohd Harithuddin, my project supervisor, which always provides guidance, support and resources towards the completion of this project. Also, to my co-supervisor, Dr Ermira Junita who provides me with useful advice and encouragement throughout the completion of this project. Not to forget, Dr Ezanee Gires for the support equipment and apparatus for the experimental setup of this project.

To all H2.1 Space System Laboratory members, Azizi Malek, Syahirah Iman, Muhammad Nazrul Adam, Muhammad Syafiq Raihan and Muhammad Amirul Fiqri, I would like to express my gratitude and appreciation for the help in terms of moral support, logistics, and manpower during conducting this project.

Finally, my sincerer gratitude to the lectures of the Faculty of Engineering, especially the Aerospace Engineering Department, who taught me for these past years and shaped me to gain sufficient skills and knowledge to further improve my skills, which is significant towards completion of this research.

This thesis was submitted to the Senate of Universiti Putra Malaysia and has been accepted as fulfilment of the requirement for the degree of Master of Science. The members of the Supervisory Committee were as follows:

**Ahmad Salahuddin bin Mohd Harithuddin, PhD**

Senior Lecturer  
Faculty of Engineering  
Universiti Putra Malaysia  
(Chairman)

**Ermira Junita binti Abdullah, PhD**

Senior Lecturer  
Faculty of Engineering  
Universiti Putra Malaysia  
(Member)

---

**ZALILAH MOHD SHARIFF, PhD**

Professor and Dean  
School of Graduate Studies  
Universiti Putra Malaysia

Date: 08 September 2022

## Declaration by Members of the Supervisory Committee

This is to confirm that:

- the research and the writing of this thesis were done under our supervision;
- supervisory responsibilities as stated in the Universiti Putra Malaysia (Graduate Studies) Rules 2003 (Revision 2015-2016) are adhered to.

Signature: \_\_\_\_\_

Name of Chairman  
of Supervisory

Committee: Dr. Ahmad Salahuddin bin Mohd Harithuddin

Signature: \_\_\_\_\_

Name of Member  
of Supervisory

Committee: Dr. Ermira Junita binti Abdullah

## TABLE OF CONTENTS

	<b>Page</b>
<b>ABSTRACT</b>	i
<b>ABSTRAK</b>	iii
<b>ACKNOWLEDGEMENT</b>	v
<b>APPROVAL</b>	vi
<b>DECLARATION</b>	viii
<b>LIST OF TABLES</b>	xiv
<b>LIST OF FIGURES</b>	xvi
<b>LIST OF ABBREVIATIONS</b>	xxv
<b>LIST OF SYMBOLS</b>	xxvii
<b>SUBSCRIPT</b>	xxx
<b>CHAPTER</b>	
<b>1 INTRODUCTION</b>	<b>1</b>
1.1 Research Background	1
1.2 Hybrid Airship UAS (HAU-3)	4
1.3 Research Objectives	5
1.4 Research Scope and Limitation	5
1.5 Thesis Organization	7
<b>2 LITERATURE REVIEW</b>	<b>8</b>
2.1 Overview	8
2.2 Hybrid Airship	8
2.3 Airship Dynamics Modelling	9
2.3.1 Newton-Euler Modelling Method	12
2.3.2 Airship Inertial Matrix	13
2.3.3 Aerostatics Buoyancy Lift	18
2.3.4 Airship Aerodynamics	20
2.3.5 Coriolis and Centripetal Effect	22
2.4 Propulsion Design and Configuration	24
2.5 UAV Dynamic Modelling and Simulation	26
2.6 Summary	28
<b>3 METHODOLOGY</b>	<b>29</b>
3.1 Overview	29
3.2 Research Workflow	30
3.3 HAU-3 Prototype Construction	32
3.3.1 HAU-3 Hull Fabrication	32
3.3.2 Hull Points of Reference Measurement	34
3.3.3 Hull Half-Profile Measurement	35
3.3.4 Thruster Configuration and Fabrication	38
3.3.5 Gondola Module and Hardware	39
3.3.5.1 Hardware Overview	40

	3.3.5.2	HAU Carrier Board Rev1.0	41
	3.3.5.3	Power Supply and Communication	43
	3.3.6	HAU-3 CAD Model	45
	3.3.7	Fully assembled HAU-3 Prototype	46
3.4		HAU-3 Dynamics Model Development	47
	3.4.1	HAU-3 Kinematic and Reference Frame	49
	3.4.1.1	HAU-3 Frame Definition	49
	3.4.1.2	Euler Angle	50
	3.4.1.3	Quaternions	52
	3.4.2	HAU-3 Inertial Matrix and Added Mass Estimation	54
	3.4.2.1	HAU-3 Physical Parameter Estimation	54
	3.4.2.2	Moment of Inertia Estimation	59
	3.4.2.3	Added-Mass Terms Estimation	60
	3.4.3	Gravity and Buoyancy Model Estimation	62
	3.4.4	Aerodynamic Model Estimation	63
	3.4.4.1	Axial Drag Coefficient	64
	3.4.4.2	Adaption of Jorgensen's Equation to HAU-3	66
	3.4.4.3	Aerodynamic Cross-Flow Estimation	69
	3.4.4.4	Resolving Aerodynamic Forces in Body-Fixed Frame	70
	3.4.5	Coriolis and Centripetal Model Estimation	72
3.5		HAU-3 Propulsion Model Estimation	72
	3.5.1	Motor and Servo Factor	73
	3.5.1.1	Horizontal and Vertical Motion	74
	3.5.1.2	Yawing Motion	75
	3.5.1.3	Pitch and Roll Motion	76
	3.5.2	Resultant Thrust	77
	3.5.3	Thruster System Identification	79
	3.5.3.1	Thruster-Motor Static Test Setup	80
	3.5.3.2	Thrust Measurement (Input PWM to Thrust)	81
	3.5.3.3	Thruster-Motor System Identification	83
	3.5.3.4	Thruster-Servo Experiment Setup	85
	3.5.3.5	Servo Minimum and Maximum input PWM	86

	3.5.3.6	Servo Voltage Feedback	87
	3.5.3.7	Thruster-Servo System Identification	88
	3.5.3.8	Propulsion Net Thrust Force and Moment	89
3.6		HAU-3 Simulator Development	91
	3.6.1	HAU-3 Simulator Block Diagram	92
	3.6.1.1	Overall Block Diagram	92
	3.6.1.2	Dynamics Model Block Diagram	93
	3.6.1.3	Apparent Mass and Inertial Matrix Subsystem	93
	3.6.1.4	Gravity and Buoyancy Subsystem	95
	3.6.1.5	Aerodynamic Subsystem	96
	3.6.1.6	Coriolis and Centrifugal Subsystem	96
	3.6.1.7	Propulsion Subsystem	97
	3.6.1.8	Quaternion and Frame Transformation	98
	3.6.2	Open-Loop Simulator	99
	3.6.3	Closed-Loop Simulator	100
3.7		HAU-3 Flight Test and Setup	103
<b>4</b>		<b>RESULTS AND DISCUSSION</b>	<b>105</b>
	4.1	Overview	105
	4.2	Thruster System Identification	105
	4.2.1	Thruster-Motor Dynamic Response Model	105
	4.2.2	Thruster-Servo Dynamic Response Model	109
	4.3	Full HAU-3 Dynamics Description	111
	4.4	HAU-3 Closed-Loop Simulator Integration	113
	4.5	Analysis of HAU-3 Simulator Response	116
	4.5.1	HAU-3 Propulsion Subsystem Response	116
	4.5.2	HAU-3 Motion Force and Moment	119
	4.5.3	Buoyancy and Gravity Subsystem	121
	4.5.4	Aerodynamic Subsystem	122
	4.5.5	Pendulum Motion	125
	4.6	HAU-3 Closed-Loop Simulator Response	126
	4.6.1	Pure Motions	126
	4.6.2	Decoupling motions	128
	4.6.3	Altitude Hold and Forward Motion	129
	4.6.4	Heading Control	130
	4.7	Flight Tests for Dynamics Parameters Validation	132

4.7.1	HAU-3 Heaviness and CG Location Test	132
4.7.2	Centre of Gravity (CG) Location test	133
4.8	Low-Level Attitude Controller Evaluation (LLC)	136
4.8.1	Case A: Pure yaw controller static test	137
4.8.2	Case B: Outdoor Dynamic Flight Test	139
<b>5</b>	<b>CONCLUSION AND FUTURE WORK</b>	<b>144</b>
5.1	Overview	144
5.2	HAU-3 Physical Prototype Development	144
5.3	HAU Dynamics Model	145
5.4	HAU Closed-Loop Simulator	145
5.5	Contribution	146
5.6	Future Work	147
	<b>REFERENCES</b>	<b>149</b>
	<b>APPENDICES</b>	<b>157</b>
	<b>BIODATA OF STUDENT</b>	<b>175</b>
	<b>LIST OF PUBLICATIONS</b>	<b>176</b>

## LIST OF TABLES

Table		Page
2.1	Summary of airship using a thruster propulsion design	24
3.1	Research phases and descriptions	32
3.2	HAU-3 airship physical parameters	35
3.3	HAU-Carrier board specifications	43
3.4	Summary of HAU-3 sub-dynamics model development approach	49
3.5	Measured data for CG location test for three different inflation pressure	56
3.6	Measured data for hull COB estimation respect to the inflation pressure	58
3.7	Parameter for $z_{CG}$ estimation via experimental	59
3.8	HAU-3 double ellipsoid and equivalent ellipsoid added mass k-factor comparison	61
3.9	HAU-3 axial drags parameters	65
3.10	Geometric parameters in aerodynamic model	70
3.11	Horizontal motion motor and servo factor	74
3.12	Vertical motion motor and servo factor	74
3.13	Yaw motion motor and servo factor	75
3.14	Pitch motion motor and servo factor	76
3.15	Roll motion motor and servo factor	76
3.16	Motor factors for all positive HAU-3 motions	77
3.17	Servo factors for all positive HAU-3 motions	77
3.18	Thruster normalized thrust definition	81
3.19	Servo shaft position respect to the PWM input	87



3.20	Estimated HAU-3 thruster position vector	91
3.21	Normalized input thrust definition	92
3.22	Closed-loop HAU-3 simulator tuned PID gain	102
4.1	First order model parameters	109
4.2	HAU-3 dynamics model parameter definition	112
4.3	Different frequency of pitch oscillation at different $z_{CG}$	125
4.4	Heaviness for case A and B heaviness test	133
4.5	CG position vector relative to the COB	134
4.6	PID-LLC gains during flight test based on HAU-3 simulator controller gains	137
4.7	Wind speed at 100 m altitude during flight test retrieved from Windy.com	139
A.1	HAU-3 mass breakdown	157
A.2	HAU-3 physical parameter estimated from experimental	157
A.3	HAU-3 dynamics parameters specifications (Used in simulator)	158
E.1	METAR data for WMSA on 16th January 2021 ( <i>Aviation Weather Center, n.d.</i> )	173
E.2	METAR data for WMSA on 17th January 2021 ( <i>Aviation Weather Center, n.d.</i> )	174

## LIST OF FIGURES

Figure		Page
1.1	Current available airships size and payload capacity ranged from small to heavy lifting airship	2
1.2	Common commercial airship. Airlander 10 (a) (Block, n.d.), Lockheed P-791 (b) ( <i>Lockheed Martin P-791 - Lockheed</i> , 2006), Goodyear Wingfoot One (c) (Goodyear, n.d.), Skyship 600 (d) ( <i>Airship Industries Skyship 600 - Airship Industries</i> , n.d.), US Navy MZ-3 airship (e) (Peek, 2013) and LZ N07-101 – Zeppelin (f) ( <i>Zeppelin NT</i> , n.d.).	2
1.3	ALTAV Quanser MkII airship (Liesk et al., 2012)	3
1.4	HAU-3 prototype	4
2.1	Dynastat hybrid airship type (Khoury, 2012)	9
2.2	Rotastat hybrid airship type (Khoury, 2012)	9
2.3	Indoor airship platform used by (Zufferey et al., 2006)	10
2.4	MkII ALTAV airship (Peddiraju et al., 2009) (Left) and AURORA airship (Moutinho, 2007)	10
2.5	Body axis convention of a conventional fin airship (left) and its body frame axis definition (right) (Carichner & Nicolai, 2013b)	13
2.6	Equivalent ellipse approximation for airship shape to estimate added mass	17
2.7	Lamb's k-factor. Adapted from (Lamb, 1918)	18
2.8	Physical prototype of airship with different thruster propulsion configuration. (a) airship model used by Navajas (2021), (b) airship model used by Peddiraju et al. (2009), (c) airship model used by Zufferey et al. (2006) and (d) airship used by Chen et al. (2015), (e) airship model used by Frye et al. (2007), and (f) Nautilus airship by Battipede et al. (2003)	25
2.9	The GT-MAB airship (Cho et al., 2017), MkII finless airship (Peddiraju et al., 2009), miniature airship with	28

sliding gondola (Alsayed, 2017), and tri-turbo fan airship prototype (Frye et al., 2007).

3.1	Illustration of the concept of grey-box model. Adapted from Duun-henriksen et al. (2013). White-box models are based mainly on knowledge about the system. Black-box models are built on statistical information from experimental data. Grey-box is the combination between white and black-box approaches.	29
3.2	Research flow chart. Reasonable open-loop response deduced based on the response of the airship towards pure motion input, such as a pure take-off motion should increase the airship altitude and climb rate.	31
3.3	HAU-3 prototype construction process	32
3.4	HAU-3 hull fabrication process flow	33
3.5	Fabricated HAU-3 hull using heat-seam method	33
3.6	HAU-3 point of reference diagram. Distance of CG from nose, $x_{cg}$ , distance of COB from nose, $x_{COB}$ , vertical distance of COB and CG, $z_{CG}$ , total length, L and maximum diameter, $d_{max}$ .	34
3.7	Hull half-profile measurement setup from side view (top) and actual experiment setup (bottom)	36
3.8	Hull half-angle profile. The solid line represented the polynomial approximation of hull profile and dashed line represented the measured hull profile via experimental.	37
3.9	Hull profile model residual error	37
3.10	HAU-3 vector thrusters' configuration in isometric view (a) and from top view (b)	38
3.11	HAU-3 thruster assembly	39
3.12	The overall HAU-3 hardware assembly	40
3.13	Gondola actual and 3D rendered model using Solid work	41
3.14	HAU-Carrier board rev1.0 top and bottom view	41
3.15	STM32F103CBT6 chip on the HAU-Carrier board	42

3.16	Here-2 GNSS receiver	42
3.17	Turnigy LiPo battery for HAU-3 power supply ( <i>Turnigy 3200mAh 4S 20C LiPoly Pack w/ EC3, 2022</i> )	44
3.18	Illustration of HAU-3 communication system that include the ground station and on-board HAU-Carrier	44
3.19	RFD 900 modem with 900MHz 2dBi straight and right-angle monopole antenna	45
3.20	Fully assembled HAU-3 CAD	45
3.21	Fully assembled HAU-3 CAD drawing (Top) and HAU-3 actual prototype (Bottom) which consisted of its three main components - Hull, thrusters' module and gondola module	46
3.22	HAU-3 dynamics modelling workflow	48
3.23	HAU-3 Frame definition	49
3.24	HAU-3 body-fixed frame definition	50
3.25	Hull CG test configuration	55
3.26	Free body diagram of bare inflated hull with air for CG test	56
3.27	COB location test configuration	56
3.28	Free body diagram of COB test	58
3.29	Procedure for the localization of $z_{CG}$ . The mass distribution along the $x$ -axis is temporarily modified, resulting in pitch angle.	58
3.30	Double ellipsoid shape estimation of HAU-3 viewed from top	60
3.31	Buoyant force $F_b$ and airship mass, $F_g$ free-body diagram COB of HAU-3 during level flight (viewed from side).	62
3.32	Buoyant force $F_b$ and airship mass, $F_g$ free-body diagram COB of HAU-3 during pitching (a) and rolling (b).	62

3.33	Drag coefficient of streamlined body against its fineness ratio, (Hoerner S.F, 1965)	66
3.34	HAU-3 aerodynamic frame definition	68
3.35	HAU Hull differential cylinder disk with a circular cross-section with different radius	69
3.36	Cross-flow around a low fineness ratio cylinder with two free-ends (Zdravkovich, Brand, Mathew, et al., 1989)	70
3.37	Thruster configuration of HAU-3. Th1 is thruster 1, Th2 is thruster 2, Th3 is thruster 3 and Th4 is thruster 4.	72
3.38	Forward (left) and vertical (right) motion free body diagram	74
3.39	Clockwise yaw motion thrust free body diagram	75
3.40	Pitch (left) and roll (right) thrust free body diagram	76
3.41	Free body diagram of resultant thrust of HAU-3	78
3.42	Flow chart of thruster system identification	80
3.43	Thruster static thrust experiment setup using RC Benchmark thrust stand	80
3.44	Block diagram of experiment setup for motor thrust measurement with PWM input	81
3.45	Normalized command input of the thruster based on PWM input	82
3.46	Thrust third order polynomial fit with 95% prediction interval.	83
3.47	Input, $u$ and output, $y$ thrust data used in black-box system identification for brushless motor. Thrust in Newton (N).	84
3.48	MATLAB System identification interface	84
3.49	Corona DS236MG servo motor	85
3.50	Vector thrust position of the thruster respect to the servo shaft angle output	85

3.51	Common servo's schematic of feedback controller with potentiometer	85
3.52	Experimental setup for servo characterization	86
3.53	Voltage feedback response of servo with shaft position (left) and the relationship of servo shaft angle with input PWM (right)	86
3.54	Ziegler-Nichol's method analysis for a step response. Adapted from (Ogata, 2010)	89
3.55	Sign convention for HAU-3 thrust in simulation (left) and the thrust vector and moment arm of the thruster (right)	89
3.56	Four main components of HAU-3	91
3.57	Simplified overall block diagram of HAU-3 Simulator	92
3.58	HAU-3 dynamics model block diagram	93
3.59	Apparent mass and inertial matrix block diagram	93
3.60	Inertial coefficient validation subsystem	94
3.61	Calculation of airship k-factor coefficient $k_1$ , $k_2$ , and $k'$ respect to its fineness ratio	94
3.62	Gravity and buoyancy block diagram	95
3.63	Pitch and roll pendulum motion frequency counter subsystem	95
3.64	HAU-3 Aerodynamic block diagram	96
3.65	Coriolis and centrifugal block diagram	96
3.66	HAU-3 propulsion block diagram	97
3.67	Overall quaternion and frame transformation Simulink subsystem	98
3.68	Overall body rates to Euler angle and DCM via quaternion terms block diagram	98

3.69	Body rates to derivative quaternion constants conversion (qdot) block diagram	99
3.70	HAU-3 open-loop simulator block diagram	100
3.71	Detailed HAU-3 dynamics block-diagram in open-loop simulator	100
3.72	Ziegler-Nichol's method of PID controller tuning.	101
3.73	HAU-3 PID controller sub-system	102
3.74	HAU-3 setup during flight test	103
3.75	HAU-3 telemetry configuration for flight test	104
3.76	HAU-3 static test setup for yaw controller evaluation	104
4.1	Estimated model response (red) against the actual thrust response (black). Validation random square wave thrust response (a) and sinusoidal validation data (b).	106
4.2	Model residual comparison between different state space model order. First order (red), second order (black) and third order (blue)	106
4.3	Estimated model step response (left) and model pole and zero (right)	107
4.4	Model validation via Simulink simulation using experimental validation data set.	107
4.5	Thruster-motor estimated model Simulink implementation block diagram.	108
4.6	Servo step response for 160° and 0° step input from horizontal position (90°). Step up response (top) and step-down response(bottom)	109
4.7	The servo dynamics model block diagram	110
4.8	Unit-step response of servo model (left) and comparison between transient response of the develop model and the actual servo response (right).	111
4.9	Simulated (black) and experimental (red) servo responses to square wave input (left) and simulated and	111

experimental servo responses to triangular wave input (right). The blue line is the input signal.

4.10	Fully integrated HAU-3 closed loop simulator	115
4.11	Closed-loop simulator input signal builder subsystem (Subsystem A)	114
4.12	Thrusters' response for five pure motion command input in open-loop simulator. Blue dashed line represents each thruster servo angle ranging from $-90^\circ$ to $90^\circ$ with default position at $0^\circ$ . Solid black line is the thrust magnitude.	118
4.13	Airship force and moment response with pure motion inputs. A section is positive vertical motion, section B represent the pitching motion, C section is the response for yawing motion and D section is the forward and backward motion force and moment response of the airship.	119
4.14	HAU-3 buoyancy subsystem dynamic response when a high and low pitch angle motion input is given. Condition of the airship is neutrally buoyant.	121
4.15	Aerodynamic subsystem response in closed-loop simulator. Region A is take-off, region B is forward motion, and region C is represented yaw.	122
4.16	HAU-2 and HAU-3 pendulum motion response in pitch during constant cruising speed of 1.0 m/s and 2.0 m/s at $z_{CG}$ location. HAU-2 case with $z_{CG}=38$ cm at $u=1$ m/s (a), and at $u=2$ m/s (b). HAU-3 case with $z_{CG}=10$ cm at $u=1$ m/s (c), and a $u=2$ m/s (d).	125
4.17	Pure motions response of HAU-3 simulator in closed-loop. All initial states are set to zero.	127
4.18	Simulated decoupling motion response when airship perform pitch and yawing while maintaining its desired altitude in closed-loop simulation.	128
4.19	Altitude holds and cruising simulation for HAU-3 using closed-loop simulation	129
4.20	HAU-3 heading control desired and actual response when airship commanded to fly at constant altitude. At $t = 200 - t = 300$ , shows the airship response when airship	131



commanded to change heading while reducing its forward speed.

4.21	Airship turning response when performing positive yaw when the airship performing forward and backward motion with a large yaw step input at low cruising speed.	131
4.22	Moment balance free body diagram during hover for determination of CG location during flight test	133
4.23	Altitude and vertical velocity data for Case A and Case B	135
4.24	Thrust and thruster angle data for Case A and Case B heaviness test	135
4.25	Outdoor flight test site. Dynamic flight test site (Right) and static flight test site (Left) located at UPM	136
4.26	Indoor yaw-controller static test response comparison between simulated and actual response.	138
4.27	Closed-up yaw response and thruster response during static test	138
4.28	Windy.com platform and with average 2kt (1.03 m/s) wind speed recorded at surface and 100 m altitude during the flight test.	140
4.29	HAU-3 Simulator and actual flight test responses comparison. Yaw motion (a), vertical motion (b), roll motion (c), pitch motion (d), forward motion (e)	141
B.1	Isometric, top and side view of HAU-3 CAD design	160
B.2	Top view of sectional cut of HAU-3	161
B.3	Bottom view of sectional cut of HAU-3	161
B.4	Unfolded sections of HAU-3 drawing using Adobe Illustrator. This section was printed on a TPU sheet and cut. Then by using heat seaming method each sections combined together to build the HAU-3's hull.	162
B.5	HAU-1 Airship prototype (Code name : PSHAU-1)	163
B.6	HAU-2 Airship prototype (Code name: Bonzo)	164

B.7	HAU-3 Airship prototype (Code name: Starway)	165
C.1	HAU Hull differential cylinder disk with a circular cross-section with different radius	166
C.2	Cross-flow Reynold number during ascend at 3 – 5 m/s.	168
C.3	Reynolds number along the airship hull for pure yaw rate 2.094 rad/s (a) and span-wise drag variation for a 3D single free-end cylinder of FR = 4 and FR = 2 (b).	168
C.4	Cross-flow around a low fineness ratio cylinder with two free-ends (Zdravkovich, Brand, Weston, et al., 1989)	169
C.5	Cross-flow drag coefficient along airship length relative to COB (a) and half-angle hull profile relative to COB (b).	171
C.6	Crossflow drag proportionality factor, $\eta$ (Jorgensen, 1973)	171

## LIST OF ABBREVIATIONS

ABS	Acrylonitrile butadiene styrene
ALTAV	Almost lighter than air vehicle
BR	Buoyancy ratio
CAD	Computer aided design
CCW	Counter clockwise rotation
CFD	Computational fluid dynamics
CG	Center of gravity
COB	Center of buoyancy
CV	Center of volume
CW	Clockwise rotation
DCM	Direct cosine matrix
DOF	Degree of freedom
ESC	Electronic speed controller
FF	Form factor
FOPD	First order plus delay
FR	Finesse ratio
GDOP	Geometric dilution of precision
GNSS	Global navigation satellite system
GPS	Global positioning system
HAU	Hybrid airship unmanned aerial system
HDOP	Horizontal dilution of precision
HLA	Heavy lifting airship

HTA	Heavier than air
IMU	Inertial measurement units
LED	Light emitting diode
LIPO	Lithium polymer
LLC	Low level controller
LTAV	Lighter-than-air vehicle
MAVLINK	Micro air vehicle link
METAR	Meteorological Aerodrome Reports
MPC	Model predictive controller
PCB	Printed circuit board
PID	Proportional, integrator and damping
PVC	Polyvinyl chloride
PWM	Pulse width modulation
RC	Radio controller
RGB	Red, green, blue
SISO	Single input, single output
STOL	Short take-off and landing
TPU	Thermoplastic polyurethane
UART	Universal asynchronous receiver/transmitter
UAV	Unmanned aerial vehicle
VTOL	Vertical take-off and landing

## LIST OF SYMBOLS

$r(x)$	Radius of the hull relative to the distance from COB
$\mathbf{M}$	Inertia matrix of the airship
$\mathbf{v}_B$	Velocities expressed in body frame
$\dot{\mathbf{v}}_B$	Acceleration expressed in body frame
$\lambda$	Rotation matrix
$\mathbf{F}_{\text{external}}$	Total external force and moment
$\mathbf{F}_R$	Restoring force and moment
$\mathbf{F}_P$	Propulsion force and moment
$\mathbf{F}_A$	Aerodynamic force and moment
$\mathbf{F}_C$	Coriolis and centripetal force and moment
$p$	Roll rate expressed in body frame
$q$	Pitch rate expressed in body frame
$r$	Yaw rate expressed in body frame
$q_0$	Quaternion constant
$q_1$	Quaternion constant 1
$q_2$	Quaternion constant 2
$q_3$	Quaternion constant 3
$\varepsilon$	Norm of the quaternion state vector
$\mathbf{x}$	Vehicle position expressed in NED
$\dot{\mathbf{x}}_B$	Vehicle velocity and rotation rates expressed in body frame
$\mathbf{M}_{\text{RB}}$	Rigid body inertia matrix
$\mathbf{M}$	Apparent inertia matrix

$\mathbf{M}_A$	Added mass inertia matrix
$\mathbf{r}_{CG}$	CG position vector
$r_{z,CG}$	Vertical position of CG relative to COB
$k_1$	Longitudinal added-mass factor
$k_2$	Lateral added-mass factor
$k'$	Ratio of apparent moment of inertia to the moment of inertia of displaced air
$I_{zh}$	Moment of inertia of the displaced air
$a_1$	Semi-major axis first ellipsoid
$a_2$	Semi-minor axis of the second ellipsoid
$a_{mean}$	Mean of semi-major axis of a double-ellipsoid
$b$	Semi-minor axis of the ellipsoid
$F_g$	Gravity force
$F_b$	Buoyancy force
$V$	Hull volume
$g$	Gravitational acceleration
$\rho_{air}$	Air density
$\rho_{He}$	Helium gas density
$\mathbf{f}$	Force matrix
$\mathbf{n}$	Moment matrix
$\boldsymbol{\eta}$	Position and orientation of the airship relative to NED
$m$	The total airship mass
$C_{D_0}$	Axial drag coefficient
$S_{ref}$	Aerodynamic drag reference area

$S_{\text{wet}}$	Wetted area for a body of revolution
$S_{C_D}$	The total drags area of the airship's hull
$C_A$	Aerodynamic axial force
$C_N$	Aerodynamic normal force
$C_M$	Pitching-moment coefficient
$\eta$	Crossflow drag proportionality factor
$A_b$	Base area
$\mathbf{v}$	Airship translational body velocity
$\boldsymbol{\omega}$	Airship rotational body rates
$\alpha$	Angle of attack
$A_p$	Planform area
$x_p$	Centroid of the planform
$T_V$	Vertical thrust
$T_h$	Horizontal thrust
$T_\phi$	Roll thrust
$T_\theta$	Pitch thrust
$T_\psi$	Yaw thrust
$T_R$	Resultant thrust
$I_{xx}$	Moment of inertia in x-direction
$I_{yy}$	Moment of inertia in y-direction
$I_{zz}$	Moment of inertia in z-direction
$I_{xy}, I_{xz}, I_{yz}$	Product of inertia
$L, M, N$	Roll, pitch and yaw moment

$\phi, \theta, \psi$	Euler angles (Roll, pitch, yaw)
$u, v, w$	Translational velocity in the body-fixed frame
$p, q, r$	Euler angle angular rate in the body-fixed frame

### SUBSCRIPT

R	Restoring force dynamics model associate
x	Surge displacement
y	Sway displacement
z	Vertical (Heave) displacement
$\phi$	Roll
$\theta$	Pitch
$\psi$	Yaw
A	Aerodynamic dynamics model associate
a.c	Aerodynamic center parameter associate
C	Coriolis and Centripetal force dynamics model associate
P	Propulsion dynamics model associate
w	Wind disturbance associate parameters
$z_{CG}$	Vertical displacement of CG respect to COB



## CHAPTER 1

### INTRODUCTION

#### 1.1 Research Background

After being neglected for a few decades, airships are now again a source of high interest, and new research programs are being launched around the world. This new airship trend is mainly due to three main reasons: A major concern for sustainable growth, increasing need for carrying heavy loads, and new expectations for survey and monitoring means. Their use represents a niche in the aeronautical market. LTAs are aerial platforms that get some or all of their lift from a lifting gas like helium, hydrogen, or hot air. Examples of this class of vehicle include airships, hot-air balloons and, tethered aerostats. There has been a resurgence of interest in Lighter-Than-Air Vehicle (LTAV) technology in recent decades, particularly in the advancement of autonomous technology in air vehicles. The rising of interest in LTA vehicle also due to its low energy consumption and long endurance capability (Li et al., 2011).

The autonomous airship, which is propelled by the buoyancy of lighter-than-air gases, has enormous potential as an aerial platform for a variety of applications including telecommunication relay, broadcasting relay, monitoring, experimental platform, and public security. Currently, most of the existing airship is classified as Heavy Lifting airship (HLA) where the payload is measured in tonnes. With the miniaturization of electronic technology, the scaling capability of airship can be improved from the HLA class to smaller design that can carry less than hundreds of kilograms of payload. Smaller airships that able to carry payloads ranging from 20-100 kg is suitable to extend the mission capacity of multi-copter drones, especially for missions that need more flight endurance and lifting capacity. The system of classification of airship size based on payload is depicted in Figure 1.1 and a commonly known commercial airship is presented in Figure 1.2.

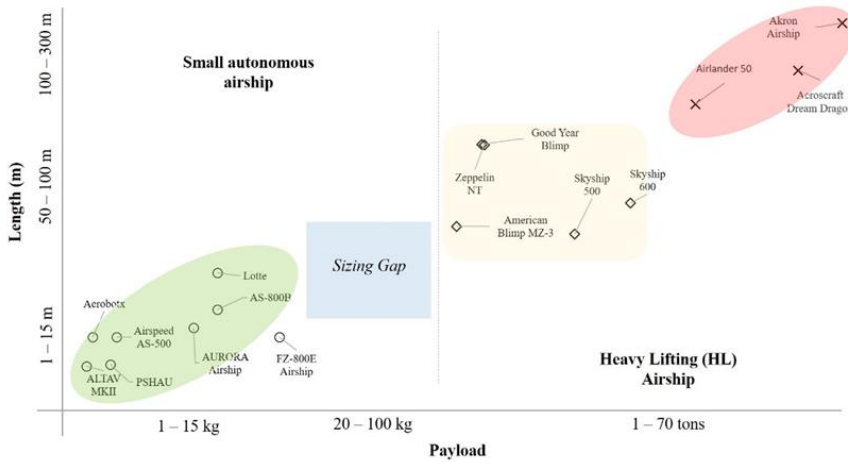


Figure 1.1: Current available airships size and payload capacity ranged from small to heavy lifting airship

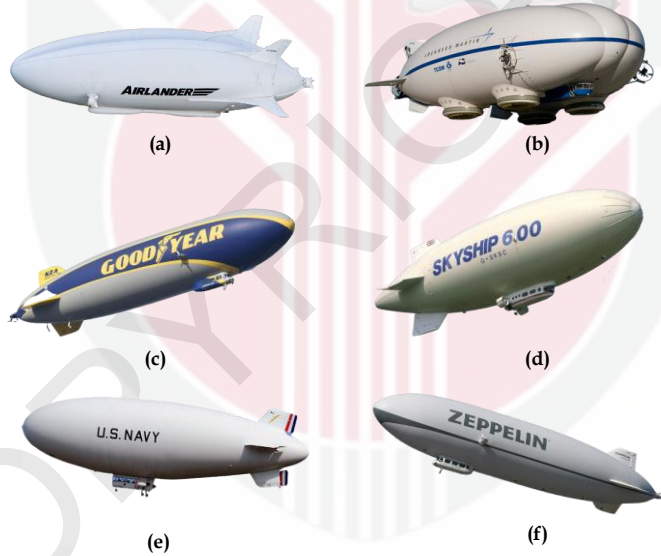


Figure 1.2: Common commercial airship. Airlander 10 (a) (Block, n.d.), Lockheed P-791 (b) (Lockheed Martin P-791 - Lockheed, 2006), Goodyear Wingfoot One (c) (Goodyear, n.d.), Skyship 600 (d) (Airship Industries Skyship 600 - Airship Industries, n.d.), US Navy MZ-3 airship (e) (Peek, 2013) and LZ N07-101 - Zeppelin (f) (Zeppelin NT, n.d.).

Currently, a major key area of interest for a buoyant vehicle is unmanned and autonomous airships. The application of this area is widely conducted all over the world, such as the ALTAV Quanser MkII that developed by Quanser Inc

(Liesk et al., 2012) as shown in Figure 1.3 these can be used for wide variety of application such as wildlife monitoring and surveillance due to the ability to relatively stealthy due to their lower heat and noise signature, aerial photography, atmospheric measurements, civil safety and security mission are major area of application.



**Figure 1.3: ALTA V Quanser MkII airship** (Liesk et al., 2012)

Due to the low mass of the typical payload, unmanned, autonomous airship is generally much smaller than airship for cargo or passenger transportation, making them more susceptible to atmospheric disturbances. As they float in the surrounding air, they tend to follow every movement of the air, such as wind gusts or thermals, unless measures are taken to counter these effects. To overcome the problem of poor ground handling and manoeuvrability at low speed, a combination between the lighter-than-air technology and the heavier than air technology such as fixed wing and rotary wing have been applied. This combination is called Hybrid Airship, the advantages of this configuration is the airship does not fully depend on the lifting gas to create lift (Khoury, 2012). The lift can be generated partially from the buoyancy force which from lifting gas and also generated dynamically from different of airflow pressure acting on the hull of the airship. Usually, the hybrid airship has unconventional shape which is the merging of several lobes body (Khoury, 2012). The application of vectored thrusters has improved the low-speed manoeuvring performance of hybrid airship which has been shown to be beneficial by number of researchers (Chen et al., 2015) (Nong, 2012). In the following section, a triangular shaped hybrid airship with axial coupling vector thrust configuration concept is presented that attempts to address the shortcomings of conventional airship design.

## 1.2 Hybrid Airship UAS (HAU-3)



**Figure 1.4: HAU-3 prototype**

The hybrid airship unmanned aerial system (HAU) is a finless airship that has a thruster configuration that enables this airship to move in biaxial direction without changing its heading. The objective of this axial-coupling thruster configuration is to improve the manoeuvrability and agility of small airships with payloads ranging from 10-100 kg. HAU-3 is the third prototype of the HAU airship series that replaced HAU-2. Its 3.3 m length, and 1.7 m hull made of lightweight material which is TPU film sheet. The vehicle consists of three major components which is the hull, thrusters and gondola as in Figure 1.4. The most distinctive feature of the HAU-3 compared to most conventional airship is its lack of aerodynamics control surface such as rudder and elevator due to its finless design. The airship becomes highly manoeuvrable in this case, but at the expense of stability due to the lack of restoring forces provided by the fins (Peddiraju et al., 2009). As a result, the airship's stability is primarily dependent on the artificial stability provided by its controller. Four vector thrusters mounted along the hull's equator provide stability control and actuation as shown in Figure 1.4. A servo tilts the motor allowing the vector thrust direction change from  $+90^\circ$  to  $-90^\circ$  make this thruster able to produce upward and downward thrust for vertical take-off (VTOL) and vertical landing. Another distinguishing feature of this airship is that, in normal operation, the airship's weight exceeds the lift generated by the helium, indicating that the airship is negatively buoyant. The excess weight will be compensated with additional lift provided by the thrusters to keep the airship airborne. The benefits of having negative buoyant are that if all of the thrusters fail, the airship will slowly sink to the ground rather than floating away with the wind, making this configuration one of its safety features.

Apart of the features that offered by this vehicle and its successful prototype construction previously, there is lack of work to understand the underlying dynamics behaviour of this vehicle. The first attempt to develop this vehicle dynamics and control system is conducted by Sedan, (2018), using a black-box modelling approach of the second HAU prototype (HAU-2). However, to develop a robust mathematical representation using experimental approach increase the project cost and duration due to the needs to conduct multiple flight test of the actual vehicle. Furthermore, the experimental approach model does not accurately represent the underlying dynamics and is only valid in the region where the vehicle is tested. In addition, to reduce the logistics cost of flight test and rapid controller design optimization a platform which enable the developed HAU-3 dynamics model to be simulated is required. The need to develop a mathematical model and a functional flight simulator in LTA and UAV vehicle study also addressed by a number of author in their work such as Alsayed (2017), Navajas (2021), Peddiraju et al. (2009) and Frye et al. (2007).

### **1.3 Research Objectives**

Hence, in order to allow a deep understanding of the HAU-3 motion behaviour and to design its attitude controller, a robust and reliable mathematical dynamics model representation and a closed-loop simulator needs to be developed.

Thus, three objectives of the research are as follows,

1. To build a working prototype of HAU-3 to be applied as a functional experimental platform.
2. To develop a six degree of freedom (6DOF) dynamics model for the HAU-3 prototype.
3. To develop closed-loop six degree of freedom (6DOF) simulator using Simulink and MATLAB for HAU-3.

### **1.4 Research Scope and Limitation**

The research work involved in the fabrication and construction of the HAU-3 airship. The airship is built from scratch based on its previous prototype design (HAU-2) that involved the fabrication of its hull, electronic board and the thruster's module. Physical parameter experiments also conducted to measure the physical parameter needed in the dynamics model. A major work involves in the development of the mathematical model of HAU-3 based on its prototype

and model implementation to build its closed-loop non-linear simulator using Simulink and MATLAB. The simulator then used to develop its flight controller. Finally, the controller and some of the dynamic parameters is validated using static and outdoor flight tests. To sum up, the scope of the research is summarized as follows:

- 1) HAU-3 prototype fabrication and assembly
- 2) Dynamics modelling of HAU-3 using Newton-Euler approach
- 3) Closed-loop simulator with PID controller development using Simulink and MATLAB
- 4) HAU-3 flight test for some of dynamics parameter validation and controller response evaluation. The test divided into two part which is static indoor test which focuses more on the evaluation of yaw controller and outdoor flight test to evaluate the controller performance and dynamics parameters validation.

In order to simplify the vehicle modelling in this research, some assumption is made before the development of HAU-3 mathematical model. The modelling assumption is as follows:

- 1) The airship hull is modelled as a rigid body, as the hull is pressurized.
- 2) The COB is the point of origin of the airship.
- 3) CG is the centre of mass of the airship.
- 4) Hull elasticity skin properties is ignored.
- 5) The airframe is symmetric about X-Z plane such that both the COB and CG lie in the plane of symmetry.
- 6) The CG is located under the COB where horizontal displacement,  $x_{CG}$  is considered relatively small and  $y_{CG}$  assumed to be zero.
- 7) Airship is neutrally buoyant in open-loop simulation. Heaviness only introduced in closed-loop simulation.

The limitation of the conducted study is laid out to provide initial insight of the study outcomes and applicability. Since the study is based on one specific vehicle design called HAU-3, thus the 6DOF mathematical model obtained from this study is applicable to HAU-3 only, however general expression of the model is still applicable for a finless airship application. Part of propulsion dynamic model is derived using black-box modelling where the model only applicable to vehicle which utilize a compatible vectored thruster configuration. The thrust mixing methodology developed in this study is specifically constructed for vehicle which utilise similar vector thruster configuration. The PID controller developed in this study is tuned based on Ziegler-Nichols's method with non-linearized plant, hence the PID gain obtained is not optimal but sufficient to make the vehicle as a functional experimental platform to analyse HAU-3

responses. HAU-3 closed loop simulator is build based on no wind disturbance assumption hence this simulator only can estimate HAU-3 states for minimal to no wind flight condition. The no wind assumption is only valid in HAU-3 simulator as the wind disturbance is not incorporated in the HAU-3 dynamics model. For actual flight test of HAU-3 prototype this ideal case is considered applicable with relatively low wind speed condition of  $<2$  m/s based on the work that conducted in this study.

## 1.5 Thesis Organization

The thesis is divided into five chapters which begins with Chapter 1 that describes the introduction of the conducted study, introduction of the vehicle used in this study and laid out of research objectives and problem statement which drives the research work. Major research related concept and previous related work is reviewed in Chapter 2.

Chapter 3 where the methodology to carried out this research is discussed in details. This chapter is divided into six sections where the first section described the overall work research flow. Section 3.2 discussed the constriction of HAU-3 prototype. The development of HAU-3 dynamics model is discussed in the third and fourth section.

The simulator construction based on dynamic model integration to SIMULINK and MATLAB is described in section five and finally the flight test setup is laid out in the last section of Chapter 3. Result and findings of the research is discussed in detail in Chapter 4, where this Chapter is divided into three major parts which is the dynamics modelling experimental result discussion.

Second part of the result, presented the finding of the developed simulator responses based on open and closed loop simulation of HAU-3 and the final part of this Chapter is a discussion on the simulator response validation based on comparison between simulation and actual vehicle response during flight test. The final Chapter of this thesis, laid out the conclusion made based on research findings and objectives also the future work recommendations.

## REFERENCES

- Abdallah, F. Ben, Azouz, N., & Beji, L. (2019). *Modeling of a heavy-lift airship carrying a payload by a cable-driven parallel manipulator*. August, 1–17. <https://doi.org/10.1177/1729881419861769>
- Air - Density and Specific Weight*. (2018). [https://www.engineeringtoolbox.com/air-density-specific-weight-d\\_600.html](https://www.engineeringtoolbox.com/air-density-specific-weight-d_600.html)
- Air - Dynamic and Kinematic Viscosity*. (2003). Engineering Toolbox. [https://www.engineeringtoolbox.com/air-absolute-kinematic-viscosity-d\\_601.html](https://www.engineeringtoolbox.com/air-absolute-kinematic-viscosity-d_601.html)
- Airship Industries Skyship 600 - Airship Industries*. (n.d.). 1984. <https://www.airliners.net/photo/Airship-Industries/Airship-Industries-Skyship-600/2042487>
- Alsayed, A. (2017). *Pitch and altitude control of an unmanned airship with sliding gondola*. University of Ottawa.
- Aviation Weather Center*. (n.d.). National Oceanic and Atmospheric Administration (NOAA). Retrieved January 16, 2021, from <https://aviationweather.gov/metar/data/>
- Azouz, N., Chaabani, S., Lerbet, J., & Abichou, A. (2012). Computation of the Added Masses of an Unconventional Airship. *Journal of Applied Mathematics*, 2012, 19. <https://doi.org/10.1155/2012/714627>
- Battipede, M., Gili, P. A., Massotti, L., & Vercesi, P. (2003). Dynamic Modelling of a Non Conventional Thrust-Vectored Airship. *AIAA Modeling and Simulation Technologies Conference and Exhibit*, August, 1–11.
- Block, I. (n.d.). “Flying bum” airship concept updated with motors powered by fuel cells alongside diesel engines. *Dezeen*. <https://www.dezeen.com/2021/06/18/airlander-electric-airship-hav-sustainable/>
- Bosma, A. (2017). *Datasheet SDP3x-Digital*. December, 1–14. [https://www.sensirion.com/fileadmin/user\\_upload/customers/sensirion/Dokumente/0\\_Datasheets/Differential\\_Pressure/Sensirion\\_Differential\\_Pressure\\_Sensors\\_SDP3x\\_Digital\\_Datasheet.pdf](https://www.sensirion.com/fileadmin/user_upload/customers/sensirion/Dokumente/0_Datasheets/Differential_Pressure/Sensirion_Differential_Pressure_Sensors_SDP3x_Digital_Datasheet.pdf)
- Boyle, A. (2018). *Egan Airships floats a sales campaign to get its Plimp hybrid aircraft off the ground*. GeekWire. <https://www.geekwire.com/2018/egan-airships-floats-sales-campaign-get-plimp-hybrid-aircraft-off-ground/>



- Carichner, G. E., & Nicolai, L. M. (2013a). *Fundamental of Aircraft and Airship Design Volume 2 - Airship Design and Case Studies* (Vol. 2). American Institute of Aeronautics and Astronautics, Inc.
- Carichner, G. E., & Nicolai, L. M. (2013b). *Fundamentals of Aircraft and Airship Design, Volume 2--Airship Design and Case Studies*. American Institute of Aeronautics and Astronautics, Inc.
- Carrión, M., Steijl, R., Barakos, G. N., & Stewart, D. (2016). Analysis of hybrid air vehicles using computational fluid dynamics. *Journal of Aircraft*, 53(4), 1001-1012. <https://doi.org/10.2514/1.C033402>
- Chen, L., Wen, Y. B., Zhou, H., Wang, X. L., Zhou, P. F., & Duan, D. P. (2015). Design and control of a multi-vector thrust airship. *22nd AIAA Lighter-Than-Air Systems Technology Conference, 2015, October*. <https://doi.org/10.2514/6.2015-3228>
- Cho, S., Mishra, V., Tao, Q., Vamell, P., King-Smith, M., Muni, A., Smallwood, W., & Zhang, F. (2017). Autopilot design for A class of miniature autonomous blimps. *1st Annual IEEE Conference on Control Technology and Applications, CCTA 2017, 2017-Janua, 841-846*. <https://doi.org/10.1109/CCTA.2017.8062564>
- Cook, M. V. (2007). *Flight Dynamics Principles*. In Elsevier Ltd. (2nd ed.). Elsevier. <https://doi.org/10.1016/B978-0-7506-6927-6.X5000-4>
- Corona DS-236MG Metal Gear Servo 7.0kg / 0.12sec / 27g. (n.d.). Retrieved January 20, 2021, from [https://hobbyking.com/en\\_us/corona-ds-236mg-metal-gear-servo-7-0kg-0-12sec-27g.html?queryID=9f3f3a23ba6efedaa94170928274c6ca&objectID=82&indexName=hbk\\_live\\_products\\_analytics](https://hobbyking.com/en_us/corona-ds-236mg-metal-gear-servo-7-0kg-0-12sec-27g.html?queryID=9f3f3a23ba6efedaa94170928274c6ca&objectID=82&indexName=hbk_live_products_analytics)
- Duun-henriksen, A. K., Sc, M., Schmidt, S., Røge, R. M., & Sc, M. (2013). Model Identification Using Stochastic Differential Equation Grey-Box Models in Model Identification Using Stochastic Differential Equation Grey-Box Models in Diabetes. *Journal of Diabetes Science and Technology*, 7(2). <https://doi.org/10.1177/193229681300700220>
- Fossen, T. I. (1987). *Nonlinear modelling and control of underwater vehicles*. Norwegian Institute of Technology.
- Fossen, T. I. (1995). *Guidance and control of ocean vehicles*. John Wiley and Sons Ltd.
- Frye, M. T., Gammon, S. M., & Qian, C. (2007). The 6-DOF dynamic model and simulation of the tri-turbofan remote-controlled airship. *Proceedings of the American Control Conference, 816-821*.

<https://doi.org/10.1109/ACC.2007.4283087>

- Funk, P., Lutz, T., & Wagner, S. (2003). Experimentelle investigations on hull-fin interferences of the LOTTE airship. *Aerospace Science and Technology*, 7(8), 603–610. [https://doi.org/10.1016/S1270-9638\(03\)00058-0](https://doi.org/10.1016/S1270-9638(03)00058-0)
- Gao, W., Nelias, D., Liu, Z., & Lyu, Y. (2018). Numerical investigation of flow around one finite circular cylinder with two free ends. *Ocean Engineering*, 156(May), 373–380. <https://doi.org/10.1016/j.oceaneng.2018.03.020>
- Goodyear. (n.d.). *Current Blimps - Wingfoot One*. <https://www.goodyearblimp.com/behind-the-scenes/current-blimps.html>
- H. Julian Allen, E. W. P. (1951). A study of effects of viscosity on flow over slender inclined bodies of revolution. *National Advisory Committee for Aeronautics (NACA), NACA-RM-A9*.
- Han, D., Wang, X. L., Chen, li, & Duan, D. P. (2016). Command-filtered backstepping control for a multi-vectored thrust stratospheric airship. *Transactions of the Institute of Measurement and Control*, 38(1), 93–104. <https://doi.org/10.1177/0142331214568237>
- Haranen, M. (2016). White , Grey and Black-Box Modelling in Ship Performance Evaluation White , Grey and Black-Box Modelling in Ship Performance Evaluation. *1st Hull Performance & Insight Conference (HullPIC), April*, 115–127.
- Helium - Density and Specific Weight. (2018). [https://www.engineeringtoolbox.com/helium-density-specific-weight-temperature-pressure-d\\_2090.html](https://www.engineeringtoolbox.com/helium-density-specific-weight-temperature-pressure-d_2090.html)
- HEX/ProfiCNC Here2 GPS. (2020). [https://docs.px4.io/master/en/gps\\_compass/gps\\_hex\\_here2.html](https://docs.px4.io/master/en/gps_compass/gps_hex_here2.html)
- Hex Cube Black Flight Controller. (2020). [https://docs.px4.io/master/en/flight\\_controller/pixhawk-2.html](https://docs.px4.io/master/en/flight_controller/pixhawk-2.html)
- Hoerner, Sighard F. (1965). Fluid dynamic drag: practical information on aerodynamic and hydrodynamic resistance. In *Copyright by: SF Hoerner Fluid Dynamics, Vancouver, Printed in the USA, Card Number 64-19666*.
- Hopkins, J., & Field, M. (1951). A semiempirical method for calculating the pitching moment of bodies of revolution at low mach numbers. In *National Advisory Committee for Aeronautics (NACA)*.
- HT 1890 Manometer. (n.d.). Retrieved January 22, 2021, from <https://hti-instrument.com/products/ht-1890-manometer>

- Hygounenc, E., Jung, I. K., Souères, P., & Lacroix, S. (2004). The autonomous blimp project of LAAS-CNRS: Achievements in flight control and terrain mapping. *International Journal of Robotics Research*, 23(4-5), 473-511. <https://doi.org/10.1177/0278364904042200>
- Jorgensen, H. (1973). Prediction of Static Aerodynamic Characteristics for Space Shuttle Like and Other Bodies At Angle of Attack From 0 degree to 180 degree. *Nasa Technical Note*.
- Kantue, P. (2018). Grey-box modelling of an Unmanned Quadcopter during Aggressive Maneuvers. *2018 22nd International Conference on System Theory, Control and Computing (ICSTCC)*, 640-645.
- Kellock, R. E., & Miller, P. H. (1971). *Aerodynamic Characteristics of Basic Nose-cylinder Bodies for Large Ranges of Angle of Attack*.
- Khoury, G. A. (2012). *Airship technology* (Vol. 10). Cambridge university press.
- Kukillaya, R. P. (2017). Simulink model development , validation and analysis of high altitude airship. *PD-FMC/2017/1000. National Aerospace Laboratories, Flight Mechanics and Control Division, Bangalore, India., March*. <https://doi.org/10.13140/RG.2.2.11844.22400>
- Lamb, H. (1895). *Hydrodynamics* (2234 (Ed.)). Princeton University Press.
- Lamb, H. (1918). The inertia coefficients of an ellipsoid moving in fluid. *Advisory Committee for Aeronautics, Reports and Memoranda No. 623, London, UK., 623*.
- Lanteigne, E., Alsayed, A., Robillard, D., & Recoskie, S. G. (2017). Modeling and Control of an Unmanned Airship with Sliding Ballast. *Journal of Intelligent and Robotic Systems: Theory and Applications*, 88(2-4), 285-297. <https://doi.org/10.1007/s10846-017-0533-6>
- Li, Y., & Nahon, M. (2007). Modeling and Simulation of Airship Dynamics. *Journal of Guidance, Control, and Dynamics*, 30(6), 1691-1700. <https://doi.org/10.2514/1.29061>
- Li, Y., Nahon, M., & Sharf, I. (2009). *Dynamics Modeling and Simulation of Flexible Airships*. 47(3). <https://doi.org/10.2514/1.37455>
- Li, Y., Nahon, M., & Sharf, I. (2011). Progress in Aerospace Sciences Airship dynamics modeling : A literature review. *Progress in Aerospace Sciences*, 47(3), 217-239. <https://doi.org/10.1016/j.paerosci.2010.10.001>
- Liesk, T., Nahon, M., & Boulet, B. (2012). Design and experimental validation of a controller suite for an autonomous , finless airship. *American Control Conference*, 2491-2496.
- Liesk, T., Nahon, M., & Boulet, B. (2013). Design and Experimental Validation of

- a Nonlinear Low-Level Controller for an Unmanned Fin-Less Airship. *IEEE Transactions on Control Systems Technology*, 21(1), 149–161.
- Ljung, L. (2011). System identification toolbox. *The Matlab User's Guide*, 1, 237.
- Ljung, Lennart. (2001). Black-box Models from Input-Output Measurements. *18th IEEE Instrumentation and Measurement Technology Conference Budapest*, 1, 138–146. <https://doi.org/10.1109/IMTC.2001.928802>
- Lockheed Martin P-791 - Lockheed. (2006). <https://www.airliners.net/photo/Lockheed/Lockheed-Martin-P-791/1153517>
- Ltd, Rfd. P. (n.d.). *Antenna 900MHz 3dBi Dipole (RPSMA)*. <https://store.rfdesign.com.au/antenna-900mhz-3dbi-dipole-rpsma/>
- Luo, S. C., Gan, T. L., & Chew, Y. T. (1996). Uniform flow past one (or two in tandem) finite length circular cylinder(s). *Journal of Wind Engineering and Industrial Aerodynamics*, 59(1), 69–93. [https://doi.org/10.1016/0167-6105\(95\)00036-4](https://doi.org/10.1016/0167-6105(95)00036-4)
- M.M. Munk. (1934). *Fluid Mechanics, 2nd Part* (In. W.F Durand (Ed.)). Julius Springer.
- Mazhar, H. (2012). *Dynamics , Control and Flight Testing of an Unmanned , Finless Airship*. McGill University, Montreal.
- Mazhar, H., Nahon, M., & Liesk, T. (2013). Validation of a dynamics model and controller for an unmanned, Finless Airship. *AIAA Lighter-Than-Air Systems Technology (LTA) Conference 2013, February*. <https://doi.org/10.2514/6.2013-1300>
- Mikegrusin, B. J. (n.d.). *Hobby Servo Tutorial*. Retrieved June 7, 2020, from <https://learn.sparkfun.com/tutorials/hobby-servo-tutorial>
- Mission Planner*. (2020). <https://ardupilot.org/planner/index.html>
- Moutinho, A. B. (2007). Modeling and Nonlinear Control for Airship Autonomous Flight. In *Praca doktorska, Universidade Técnica de Lisboa, Lisboa, Grudzień*. <https://doi.org/10.13140/2.1.1333.8568>
- Mueller, J., Paluszek, M., & Zhao, Y. (2004). Development of an aerodynamic model and control law design for a high altitude airship. *AIAA 3rd "Unmanned Unlimited" Technical Conference, Workshop and Exhibit*, 6479.
- Munk, M. M. (1931). The aerodynamic forces on airship hulls. In *National Advisory Committee for Aeronautics* (Vol. 211, Issue (No. NACA-TR-184)). [https://doi.org/10.1016/s0016-0032\(31\)90371-2](https://doi.org/10.1016/s0016-0032(31)90371-2)

- Navajas, G. T. (2021). *Modelling and Pitch Control of a Re-configurable Unmanned Airship*. University of Ottawa.
- Nicolai, L. M., & Carichner, G. E. (2010). *Fundamentals of aircraft and airship design, volume 1--aircraft design*. American Institute of Aeronautics and Astronautics.
- Nong, Y. (2012). *Design of Small Highly Maneuverable Airships*. McGill University, Department of Mechanical Engineering.
- Ogata, K. (2010). *Modern Control Engineering* (Fifth). Pearson Education Inc.
- Pais, A. R., & Pais, A. R. (2006). *Project AURORA : Infrastructure and Flight Control Experiments for a Robotic Airship*. 23(December 2005), 201–222. <https://doi.org/10.1002/rob>
- Park, S. (2013). *RFD900 Radio Modem Data Sheet*. <http://files.rfdesign.com.au/Files/documents/RFD900 DataSheet.pdf>
- Paul Scherz, & Monk, S. (2016). *Practical Electronics for Inventors* (Fourth). McGraw-Hill Education.
- Peddiraju, P. (2010). *Development and validation of a dynamics model for an unmanned finless airship*. McGill University.
- Peddiraju, P., Liesk, T., & Nahon, M. (2009). Dynamics modeling for an unmanned, unstable, fin-less airship. *18th AIAA Lighter-than-Air Systems Technology Conference, May*. <https://doi.org/10.2514/6.2009-2862>
- Peek, D. (2013). *Navy manned airship lands at Dobbins*. 94th Airlift Wing Public Affairs. <https://www.dobbins.afrc.af.mil/News/Article-Display/Article/561962/navy-manned-airship-lands-at-dobbins/>
- Peterson, M. A. (2002). Galileo's discovery of scaling laws. *American Journal of Physics*, 70(6), 575–580. <https://doi.org/10.1119/1.1475329>
- RFD 900+ Modem*. (n.d.). Retrieved January 22, 2021, from <https://store.rfdesign.com.au/rfd-900p-modem/>
- S. B. V. Gomes. (1990). *An Investigation of the Flight Dynamics of Airships with Application to the YEZ-2A*. Cranfield Institute of Technology.
- Sagatun, S. I., & Fossen, T. I. (1991). Lagrangian formulation of underwater vehicles' dynamics. *Proceedings of the IEEE International Conference on Systems, Man and Cybernetics*, 2, 1029–1034. <https://doi.org/10.1109/icsmc.1991.169823>
- Sebbane, Y. B. (2019). *Lighter Than Air Robots Guidance and Control of Autonomous Airships* (Vol. 53, Issue 9). Springer.

<https://doi.org/10.1017/CBO9781107415324.004>

Sedan, M. F. (2018). *Flight Control System Performance Analysis of Finless Hybrid Airship (PSHAU-2)*. Universiti Putra Malaysia.

Series 1585 Test Stand Datasheet. (2022). Tyto Robotics. [https://cdn.rcbenchmark.com/landing\\_pages/Manuals/Series\\_1585\\_Datasheet.pdf](https://cdn.rcbenchmark.com/landing_pages/Manuals/Series_1585_Datasheet.pdf)

STM32F103x8, STM32F103xB. (2022). <https://www.st.com/resource/en/datasheet/stm32f103c8.pdf>

Tischler, M. B., Ringland, R. F., & Jex, H. R. (1983). Heavy-Lift Airship Dynamics. *Journal of Aircraft*, 20(5), 425–433.

TPS56637 4.5-V to 28-V input, 6-A Synchronous Buck Converter. (2019). [https://www.ti.com/lit/ds/symlink/tps56637.pdf?ts=1619973800610&ref\\_url=https%253A%252F%252Fwww.google.com%252F](https://www.ti.com/lit/ds/symlink/tps56637.pdf?ts=1619973800610&ref_url=https%253A%252F%252Fwww.google.com%252F)

Tuckerman, L. B. (1926). *Inertia factors of ellipsoids for use in airship design*.

Turnigy 3200mAh 4S 20C LiPoly Pack w/ EC3. (2022). [https://hobbyking.com/en\\_us/turnigy-3200mah-4s-20c-lipoly-pack-w-ec3-e-flite-compatible-eflb32004s.html?queryID=c0dc728da04eff5c481ff62d9c4367e0&objectID=45413&indexName=hbk\\_live\\_products\\_analytics](https://hobbyking.com/en_us/turnigy-3200mah-4s-20c-lipoly-pack-w-ec3-e-flite-compatible-eflb32004s.html?queryID=c0dc728da04eff5c481ff62d9c4367e0&objectID=45413&indexName=hbk_live_products_analytics)

Tuveri, M., Ceruti, A., & Marzocca, P. (2014). Added masses computation for unconventional airships and aerostats through geometric shape evaluation and meshing. 15(3), 241–257. <https://doi.org/10.5139/IJASS.2014.15.3.241>

Windy.com. (n.d.). Retrieved January 16, 2021, from <https://www.windy.com>

Zdravkovich, M. M., Brand, V. P., Mathew, G., & Weston, A. (1989). Flow past short circular cylinders with two free ends. *Journal of Fluid Mechanics*, 203.

Zdravkovich, M. M., Brand, V. P., Weston, A., & Mathew, G. (1989). Flow past short circular cylinders with two free ends. *Journal of Fluid Mechanics*, 203(557), 557–575. <https://doi.org/10.1017/S002211208900159X>

Zeppelin NT. (n.d.). Airships.Net. <https://www.airships.net/zeppelin-nt/>

Zhang, L., Lv, M., Sun, C., & Meng, J. (2018). Flight performance analysis of hybrid airship considering added mass effects. *Journal of Dynamic Systems, Measurement and Control, Transactions of the ASME*, 140(11), 1–13. <https://doi.org/10.1115/1.4040220>

Zufferey, J. C., Floreano, D., Van Leeuwen, M., & Merenda, T. (2002). Evolving vision-based flying robots. *Lecture Notes in Computer Science (Including*

*Subseries Lecture Notes in Artificial Intelligence and Lecture Notes in Bioinformatics*), 2525, 592–600. [https://doi.org/10.1007/3-540-36181-2\\_59](https://doi.org/10.1007/3-540-36181-2_59)

Zufferey, J. C., Guanella, A., Beyeler, A., & Floreano, D. (2006). Flying over the reality gap: From simulated to real indoor airships. *Autonomous Robots*, 21(3), 243–254. <https://doi.org/10.1007/s10514-006-9718-8>

